

Characteristics of Extended-Gate Field-Effect Transistor (EGFET) Based on Porous *n*-Type (111) Silicon for Use in pH Sensors

NASER M. AHMED,^{1,2} E.A. KABAA,¹ M.S. JAAFAR,¹ and A.F. OMAR¹

1.—Universiti Sains Malaysia, Gelugor, Penang, Malaysia. 2.—e-mail: nas_tiji@yahoo.com

Following the advances in pH sensors based on porous silicon (p-Si) in the late 20th century, several studies have been carried out to take advantage of the intrinsic properties of p-Si for development of chemical sensors. This study investigates the characteristics and pH sensitivity of an extended-gate field-effect transistor (EGFET) based on *n*-type p-Si with (111) orientation. Porous silicon was applied directly without coating. The x-ray diffractogram revealed only *n*-type (111) crystal orientation. p-Si was comparatively analyzed against a silicon wafer (flat and porous surface) in the pH range from 2 to 12. Regarding EGFET operation, p-Si exhibited significantly enhanced pH sensitivity of 56.13 mV/pH and linearity of 0.9857 (at drain–source current I_{DS} of 0.1 mA, temperature of 300 K, and immersion time of 300 s) because of its high surface area, whereas the silicon wafer (flat and porous surface) exhibited comparatively poor sensitivity of 25.41 mV/pH and linearity of 0.99 under similar conditions. In addition, we demonstrate use of current as a second parameter with high linearity for pH sensing. The low hysteresis depth (9 mV) of the EGFET sensor based on p-Si indicates good stability and reversibility.

Key words: Porous silicon, EGFET, silicon, pH sensor, sensitivity, hysteresis

INTRODUCTION

The extended-gate field-effect transistor (EGFET) structure has attracted much attention in terms of packaging and passivation because of its insensitivity to light and temperature, as well as its flexible extended gate. Moreover, EGFETs can be used without the metal–oxide–semiconductor field-effect transistor (MOSFET) coming into contact with the solution, enabling its reuse several times.¹ The EGFET configuration allows separation of the MOSFET from the biological or chemical environment.² The MOSFET is formed by connection of a sensing membrane to the end of a signal line.² In addition, this configuration provides a larger detection region by enabling use of larger-size samples without being restricted by the size of the MOSFET.

In pH sensing, the surface potential is controlled by a physical protonation/deprotonation reaction at the membrane surface.³ Adsorbed ions modify the surface potential (SP). The SP difference between the electrolyte and gate results in an electric field at the semiconductor interface, consequently modifying the field-effect transistor (FET) channel conductance and the drain–source current (I_{DS}). Measuring I_{DS} is less complex and faster when the SP varies at the surface of the membrane.^{4,5}

The nanostructure of porous silicon (p-Si) is influenced by current density, type and dopant concentration of the silicon wafer used, temperature, electrolyte composition, light intensity, surface tension, molecular weight, dimensions, and dipole moment. p-Si has recently been used as a novel transducer material for chemical sensors and biosensors. Anodic etching can be applied to fabricate semiconducting p-Si for use in sensors. Use of p-Si has several advantages: p-Si with varying pore sizes ranging from nanoporous (less than 2 nm) to

macroporous (more than 50 nm) can be produced by controlling the etching parameters. The amount of sensing sites can be increased by increasing the surface area. p-Si has increased surface area exceeding $100 \text{ m}^2/\text{m}^3$, approximately a thousand times greater than a polished silicon surface.⁷ Also, it does not require addition of a passivation layer for electronic components on the sensor chip. Moreover, p-Si is mechanically stable due to the presence of ions inside its pores, which prevent leakage.⁶

The intrinsic properties (resistance, capacitance, optical reflectivity, and photoluminescence) of p-Si make it an appropriate precursor material for manufacture of detectors for liquid and gaseous analytes such as toxins, explosives, polycyclic aromatic hydrocarbons, volatile organic compounds, deoxyribonucleic acid (DNA), and proteins.⁸ Moreover, its simplicity, rapid manufacture, morphological and optical properties (including porosity and controlled pore size), adjustable internal surface area, and multifaceted surface chemistry make p-Si a prominent nanostructured material for use in biological sensors.⁹

MORPHOLOGICAL CHARACTERISTICS OF p-Si

Given the difficulty of obtaining an accurate quantitative description, it is extremely challenging to characterize the morphology of p-Si systematically because of the different ranges of pore size, orientation, shape, interconnection, distribution, and branching. When using electrochemical etching, the resulting morphology depends on the illumination and doping concentration, while the size is directly proportional to the doping concentration for *p*-type Si and inversely so for *n*-type Si. The key factors that influence the pore shape include the crystallographic orientation and doping density, whereas the current density (as a function of charge transfer) strongly influences the pore size.¹⁰ The $\langle 100 \rangle$ direction requires the smallest number of holes per silicon atom, so this

crystallographic orientation is preferred for charge transfer. For (111) orientation, the path diverts to $\langle 113 \rangle$ direction, because the growth velocity of pores for $\langle 113 \rangle$ direction is faster vertically to the surface than $\langle 100 \rangle$ direction. This elucidates a triangular sectional form for (111) direction but square section for (100).¹¹ The thickness of the p-Si layer varies linearly with the charge transferred. Nonetheless, the pore size is the most important parameter to characterize the morphological features as well as the physical and chemical properties of porous silicon, due to the simplicity of its measurement.¹² The pore size of low-doped silicon has been observed to be larger than for high-doped silicon, thus pore size is directly proportional to the resistivity of the silicon wafer.¹⁰

The increased surface-to-volume ratio (via a rough surface) for smaller dimensions (sizes) increases the sensitivity, because the sensing part is exposed to more effective control by the electrolyte. Small dimensions provide better conductivity, while large dimensions remain unaffected by buffer solution in the dipped area. This behavior is likewise reflected in the threshold shift between different hydrogen ion (H^+) concentrations in the buffer solution.¹³ Calculations using the theoretical site-binding model are based on a smooth flat surface.¹⁴ Meanwhile, inhomogeneities will predominantly alter the dimensions of the surface, which is not predicted by the model. The sensing response is a function of charged particle size. For noncomplex infiltration, their Debye length must be considerably smaller than the pore diameter. In contrast, infiltration of ions of larger diameter into pores is more difficult. Some studies have shown that the pore diameter has to be five- to tenfold greater than the charged molecule diameter, suggesting greater sensitivity for decreasing pore size.^{15,16} Researchers have similarly inferred that more distinct pores with larger and deeper dimension will increase the sensitivity by increasing the strength of the electric field (at the bottom of pore), resulting in a change in the current-voltage (I - V) characteristic.¹⁷

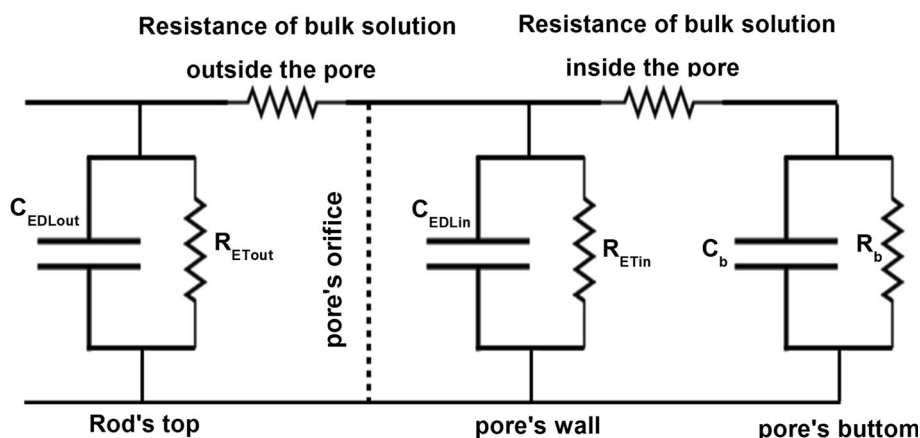


Fig. 1. Equivalent electrical circuit for the reaction between electrode and electrolyte.

The objective of this study is to apply H^+ sensing to determine pH in the range from 2 to 12 using EGFETs based on a flat surface or p-Si. In addition, the pH sensing responses of smooth flat silicon and p-Si are comparatively analyzed.

POROUS ELECTRODE-ELECTROLYTE INTERFACE

There are two explanations for the modification of the electrical conductivity observed for a porous structure. The first is based on alteration of the charge distribution within crystallites due to

orientational ordering of polar molecules on the surface. The second is based on the notion that holes serve as traps that capture ions during physical adsorption and ion oxidation, thus inhibiting or impeding physical desorption.¹⁸ Electrostatic equilibrium occurs at the solid-liquid interface after the electrolyte overflows to the porous layer. This electrostatic equilibrium creates an electrical double layer (EDL) between the space-charge region (SCR) of Si and the electrolyte (Helmholtz layers) to generate an electric field. The Helmholtz region is formed by adsorbed ions on the surface and lies between the two layers. The potential (Galvani

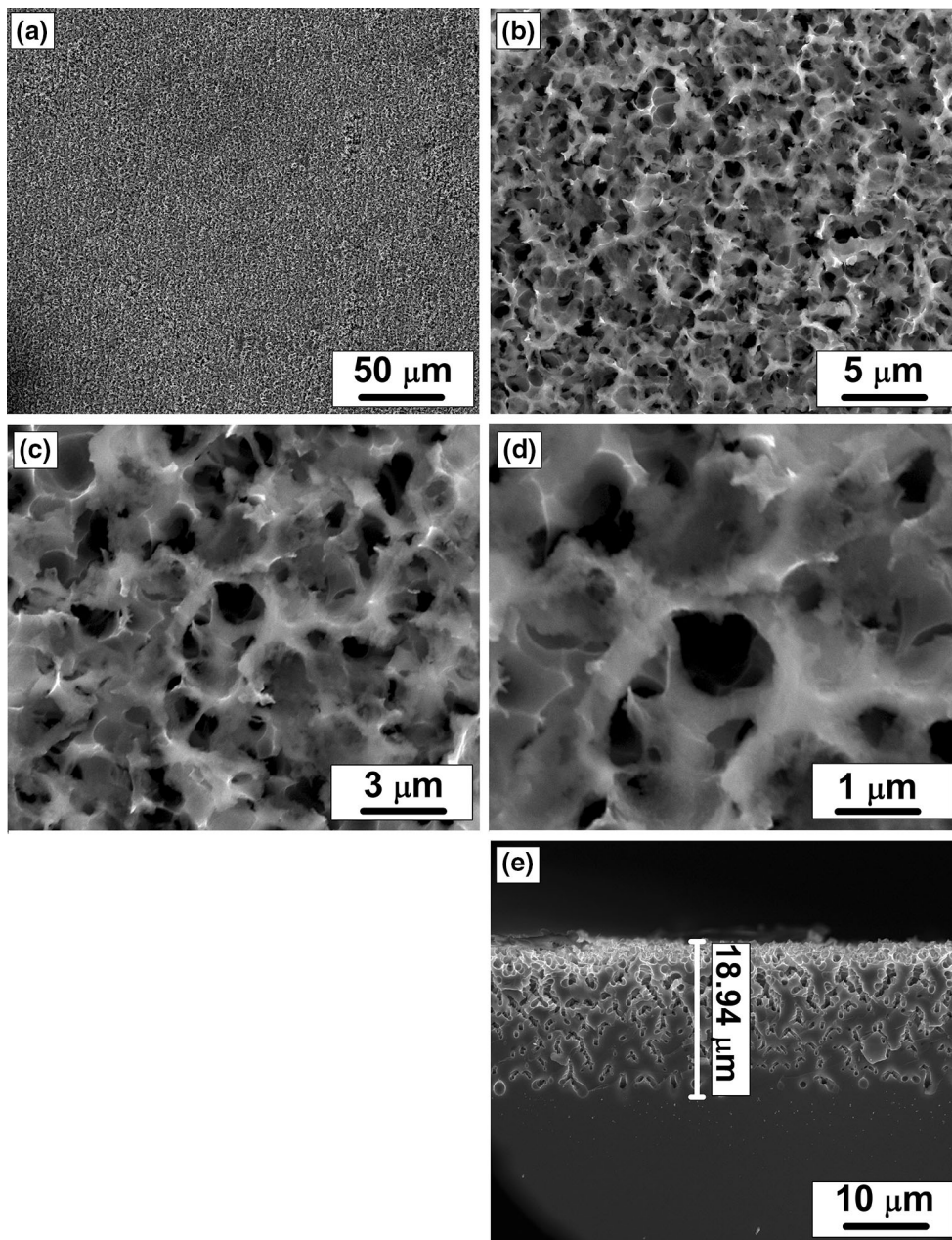


Fig. 2. FESEM micrographs of p-Si at (a) 1000 \times , (b) 10,000 \times , (c) 25,000 \times , (d) 50,000 \times , and (e) cross-section of p-Si layer at 5000 \times .

potential) declines across the EDL. The Helmholtz region is strongly influenced by the components and concentration of the electrolyte and the physical adsorption/desorption of ions. Electrostatic equilibrium is attained through the compensating ion process.¹⁹

The structure of the porous layer comprises net-connected crystalline Si pillars standing on a crystalline Si substrate, interposed by holes extending vertically from the surface in the direction of the substrate. As mentioned above, the solution comes into contact with three regions: the tops of the pillars, walls, and bottoms of pores. The bottom of the pore is the closest to the bulk layer.²⁰ The potential difference across the EDL inside the pore results in current transfer as a function of position and time along the direction of the pore's bottom. The homogeneity of the distribution of the current density depends on time, the electrolyte concentration, the EDL capacitance of the pore, and the electron transfer reaction.²¹

In the case of *n*-type (111) Si, the shape of the pore is similar to an inverted cone. The disparity between the diameter of macropores and nanopores results in fixed placement of ions at a specific location within the pore, which is appropriate for the Debye length of the ion. This creates a potential difference inside the pore. The voltage between the Stern (Helmholtz) layer and the electron-conducting matrix produces an electrical bridge between the macropore and the electron-conducting matrix. Local electroneutrality in the macropores arises through the matched ion concentrations, whereas the electrons and chemical charge account for the local charge balance on the nanoscale.^{22,23} Ions contained in the layers of the EDL (from the weak to Stern layer) are only conveyed on the macroscale. This effect is vital to generate a surface charge density close to stability, which is enhanced when the thickness of the EDL approximately equals the pore depth, thus strongly depleting the electrolyte.^{24,25} In effect, variation in the constituents of the electrolyte can affect its electrical connectivity (Fig. 1).

EXPERIMENTAL PROCEDURES

An *n*-type Si wafer (111 orientation) was divided into small pieces with dimensions of 2.4 cm × 2.4 cm. All pieces were cleaned using the Radio Corporation of America (RCA) method. Ethanol/HF solution (4:1 mixture) was used to form a p-Si layer by anodic etching with current density of 8.5 mA/cm² and anodization time of 15 min under 100 W of illumination at 300 K, followed by washing with ethanol, as shown in Fig. 2. The pore diameter of macroporous type according to the International Union of Pure and Applied Chemistry (IUPAC) classification²⁶ was in the range of 250 nm to 750 nm for p-Si layer thickness of 18.94 μm. Images of the surface morphology of p-Si were acquired

by field emission scanning electron microscope (FESEM, FEI Nova NanoSEM 450) at 10 keV.

The crystalline properties were examined by x-ray diffraction analysis (Philips X'Pert high-resolution x-ray diffractometer with Cu K_α radiation with wavelength of 0.15419 nm). Figure 3 shows a distinctive high peak at $2\theta = 28.375^\circ$, indicating (111) plane of Si.²⁷

The two parts of an EGFET are the sensing component (Si) and a commercial MOSFET (CD4007UB). The Si-based EGFET pH sensor is depicted in Fig. 4. Two samples were tested to comparatively analyze their response to H⁺ and hydroxide ions (OH⁻) and investigate the effects of the porous structure on the pH sensitivity. The first sample had a smooth (flat) surface, whereas the other had a p-Si layer. The sensing part of the sensor was connected to the MOSFET's gate. The sensing membrane and an Ag/AgCl reference electrode were immersed in pH buffer solution and subsequently connected to the measurement system. Each pH value was measured twice after immersion times of 1 min and 5 min. The first immersion period of 1 min (60 s) stabilized the signal, while the second duration of 5 min allowed further stabilization for each new test. The response of the sensor was analyzed using a Keithley 2400 with Lab Tracer 2 software. Six pH buffer solutions obtained from Titrisol[®] were used in the pH test range from 2 to 12.

RESULTS AND DISCUSSION

Generally, the surface of a FET channel can adapt to the surface charge at given pH. The conductivity of the FET channel changes depending on whether the charge is negative or positive. In this study, *n*-type Si was selected as the device layer to examine the accumulation of the EGFET. Therefore, introducing a positive surface charge increases the concentration of carriers in the

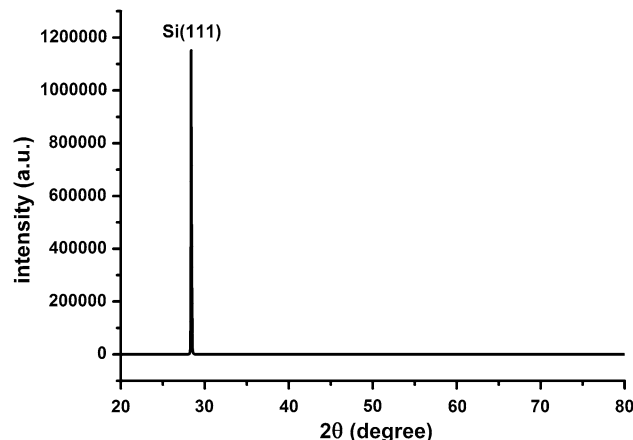


Fig. 3. XRD spectrum with single sharp peak at $2\theta = 28.375^\circ$ denoting only silicon (111) plane.

channel, while addition of negative charge drains the channel.

Based on the site-binding model, in the saturation region, there is a voltage difference between the

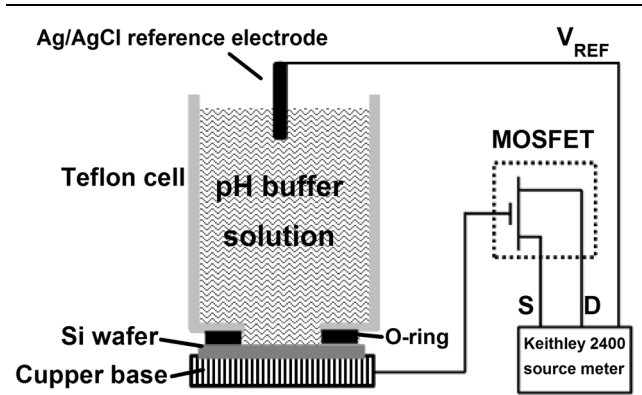


Fig. 4. Schematic diagram of porous Si pH sensor measurement system.

working electrode (negative) and the cations (hydrogen ions), which results in movement of H^+ ions to the negative sensing surface (Si) while OH^- ions move to the reference electrode.²⁸ This phenomenon provides a plausible explanation for the greater current recorded for more acid solutions (low pH). I_{DS} adjusts to the corresponding gate voltage with increasing H^+ concentration.

Figures 5b, e and 6b, e illustrate the negative relation between I_{DS} and the pH value that was measured for the two sample EGFET pH sensors. The reference voltage (V_{Ref}) was set at 3 V based on the current sensitivity. The current sensitivity of the EGFET pH sensors was measured at corresponding drain-source voltage (V_{DS}) of 4 V. The different pH values of the buffer solutions correspond to the H^+ ion concentration (caused by the positive gate bias), resulting in a linear change of I_{DS} .

The results above validate the possibility of using the I_{DS} sensitivity of silicon pH sensors to augment their V_{Ref} sensitivity. Figures 5a, d and 6a, d show the $I_{DS}-V_{DS}$ characteristic of the EGFET in the pH

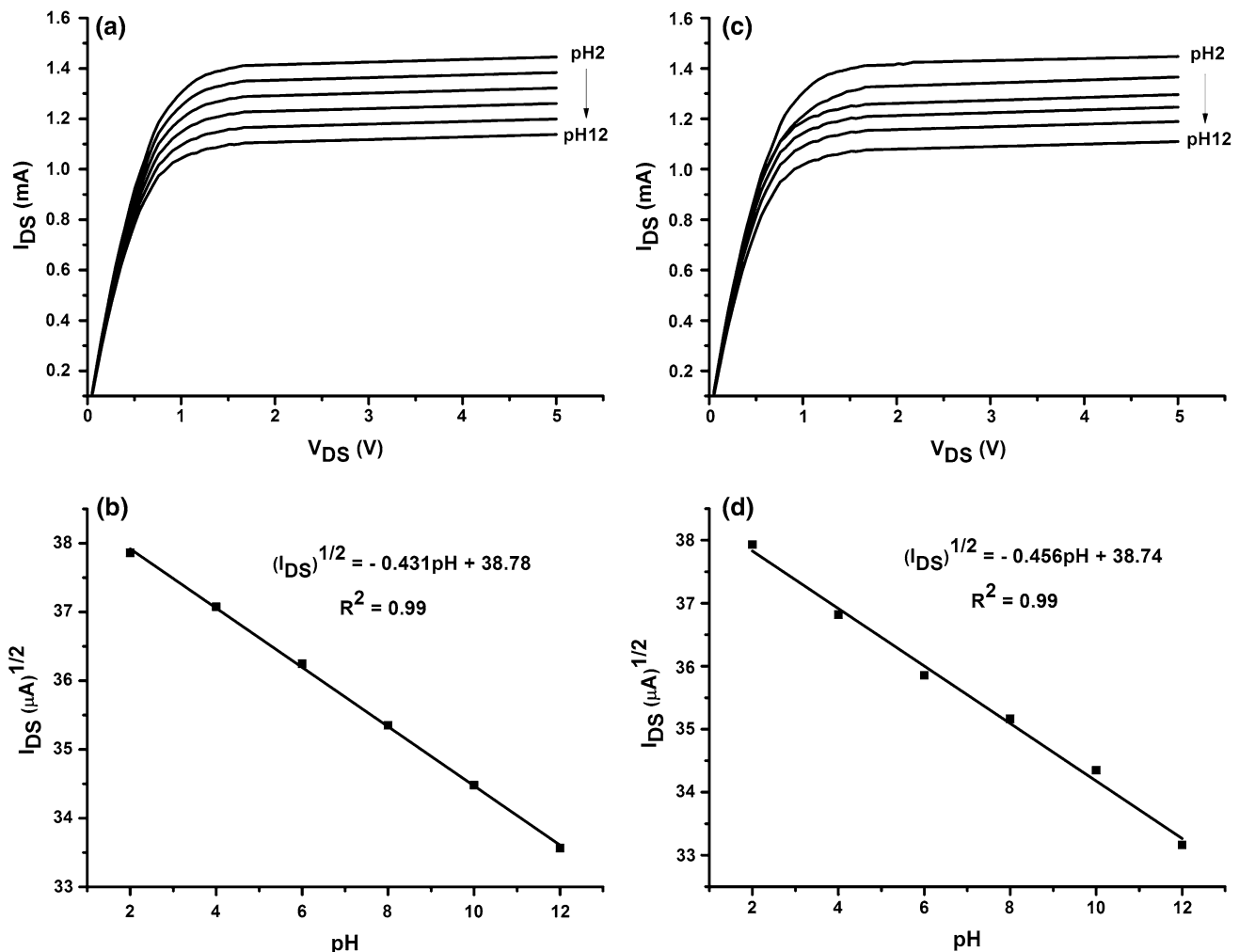


Fig. 5. $I_{DS}-V_{DS}$ characteristics of EGFET with flat Si for two immersion periods of 60 s and 300 s: (a) $I_{DS}-V_{DS}$ characteristic for 60 s, (b) $\text{sqrt}(I_{DS})-\text{pH}$ characteristic for 60 s, (c) $I_{DS}-V_{DS}$ characteristic for 300 s, and (d) $\text{sqrt}(I_{DS})-\text{pH}$ characteristic for 300 s.

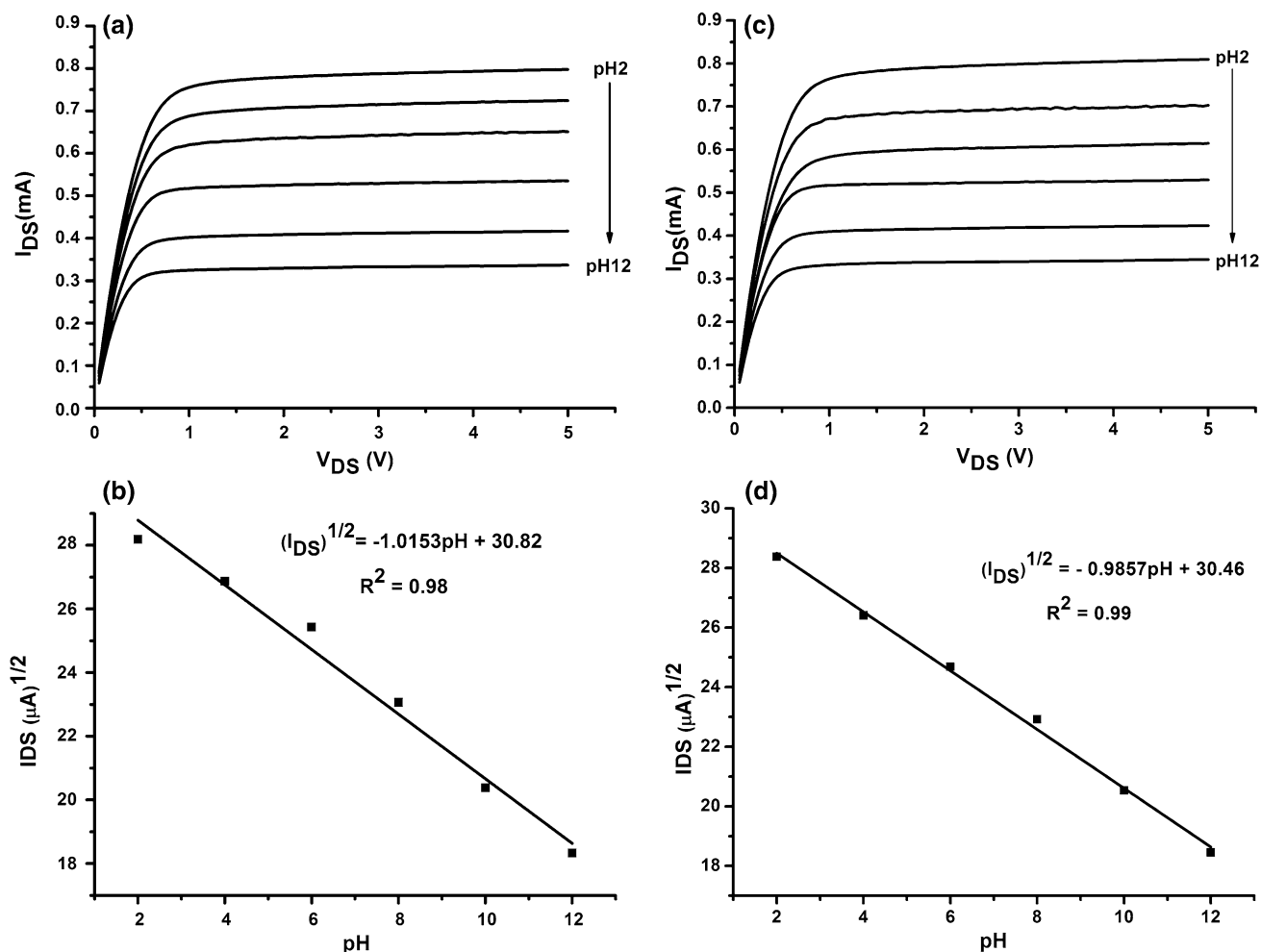


Fig. 6. I_{DS} - V_{DS} characteristics of EGFET with p-Si for two immersion periods of 60 s and 300 s: (a) I_{DS} - V_{DS} characteristic for 60 s, (b) $\sqrt{I_{DS}}$ -pH characteristic for 60 s, (c) I_{DS} - V_{DS} characteristic for 300 s, and (d) $\sqrt{I_{DS}}$ -pH characteristic for 300 s.

buffer solutions discussed above. The current in the saturation region can be expressed using the following equation²⁹:

$$\sqrt{I_{DS}} = \sqrt{\frac{\mu_0 C}{2} \times \frac{W}{L} \times (1 + \lambda V_{DS})(V_{Ref} - V_T)}, \quad (1)$$

where μ_0 is the electron mobility in the channel, λ is the factor modulation of channel length, C is the gate capacitance per unit area, W/L is the width-to-length ratio of the channel, V_T is the threshold voltage of the EGFET sensor, and V_{DS} and V_{Ref} denote the drain-source voltage and applied reference electrode voltage, respectively.

In the linear region, the relationship between I_{DS} and V_{Ref} can be expressed as follows³⁰:

$$I_{DS} = \sqrt{\frac{\mu_0 C W}{2 L}} [2(V_{Ref} - V_{T(EGFET)})V_{DS} - V_{DS}^2]^2. \quad (2)$$

Figures 7a, c and 8a, c reveal a positive correlation between I_{DS} and V_{Ref} in the linear region at

$V_{DS} = 0.3$ V for flat silicon and p-Si, respectively. The increase of V_{Ref} concomitantly increases the current due to increased dissociation of OH^- ions; i.e., the rise in the pH value produces V_{Ref} . The decline of I_{DS} resulting from the decrease of H^+ can be attributed to the negative bias on the gate. V_{Ref} then has to increase with increasing pH value to maintain the I_{DS} value. The linear correlation between V_{Ref} and pH is shown in Figs. 7b, d and 8b, d. The pH sensitivity was calculated at $I_{DS} = 0.1$ mA to 0.6 mA and 0.1 mA to 0.4 mA for flat silicon and p-Si, respectively, in the pH range from 2 to 12.

Changing the solution pH modifies the state (electrical conductivity) of the sample, resulting in failure of the sensor in real-time measurements, since the tested buffer solutions had various ion concentrations.⁵ This may be the effect of the rate-limiting step of the reaction between H^+ and the sensing part of the EGFET. This measurement error and other inherent features of the silicon wafer such as drift potential and hysteresis potential affected the reliability of the pH sensitivity values.³¹

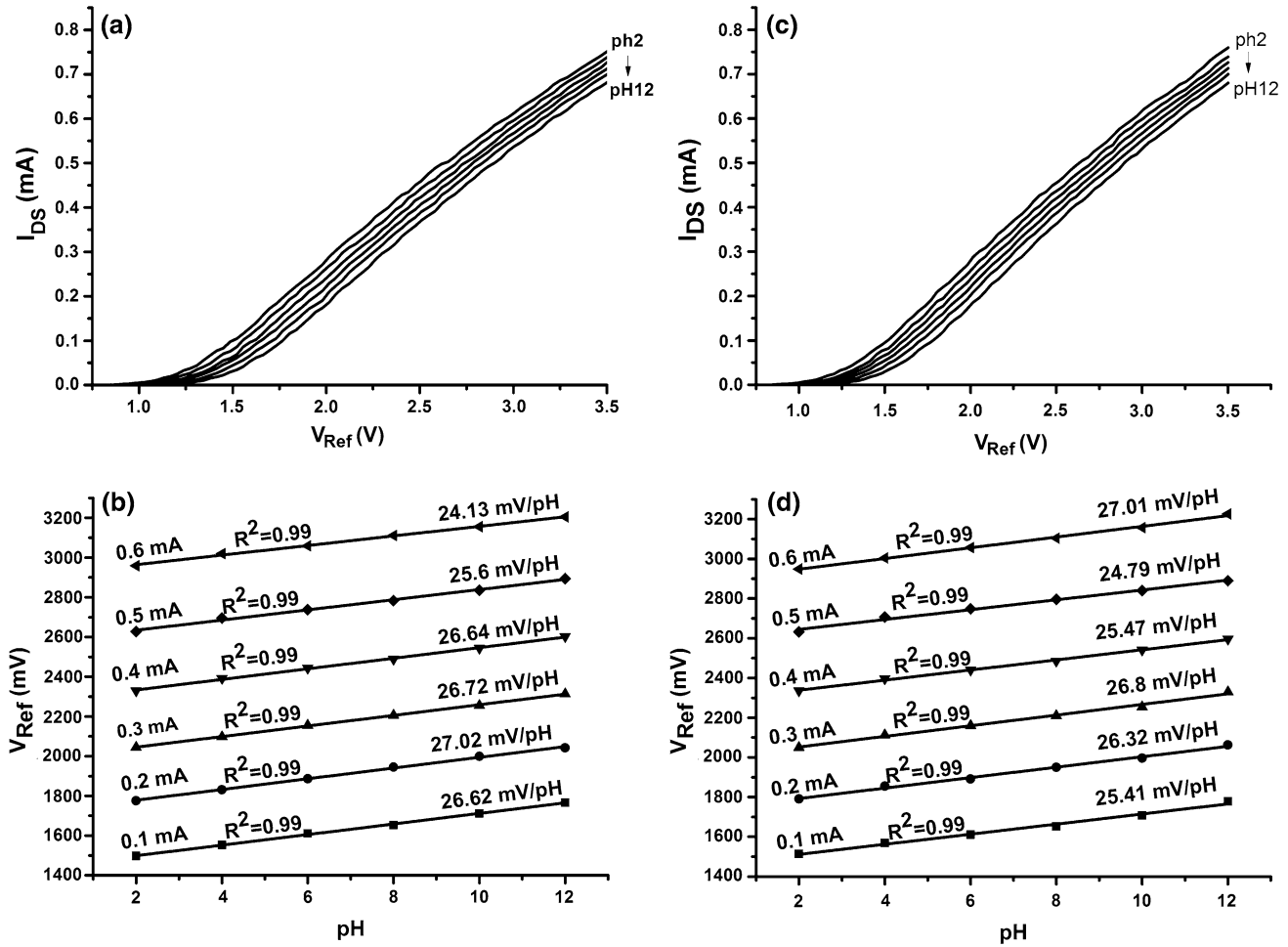


Fig. 7. I_{DS} - V_{Ref} characteristics of EGFET with flat Si for two immersion periods of 60 s and 300 s: (a) I_{DS} - V_{Ref} characteristic for 60 s, (b) V_{Ref} -pH characteristic for 60 s, (c) I_{DS} - V_{Ref} characteristic for 300 s, and (d) V_{Ref} -pH characteristic for 300 s.

Given its larger connected surface area and higher number of sites per unit, the sensitivity of the p-Si device was closer to the ideal Nernst value (59 mV/pH at 297 K) compared with the flat Si device.³² This explains the effects of their different surface morphologies on the reference voltage in terms of modifying the membrane conductivity. Al-Hardan et al.³² investigated the pH sensing capacity of an EGFET based on *n*-type (100) p-Si. Their results revealed excellent pH sensitivity of 66 mV/pH in the pH range from 2 to 12 at 298 K. That study attributed the high pH sensitivity to the porous nature of p-Si. Porosity enhances pH sensitivity by increasing charge accumulation, resulting in higher current. Reddy et al.³³ and Thust et al.³⁴ reported pH sensitivity of 30 mV/pH for *n*- and *p*-type (100) porous silicon, respectively, for the pH range from 3 to 10. The results of the cited studies are consistent with the notion that the FET is advantageous for manufacture of such biochemical sensors.³⁵

Furthermore, the pores of porous *n*-type (111) silicon are conical in shape and characterized by a

sponge-like structure (Fig. 2). The pore lengthens sideways, like branches (barb effect). The narrow diameter of the pore bottom ensures confinement and restriction of ions, leading to increased stability of their physical adsorption.³⁴ In addition, the abundance of lateral branches in p-Si (111) increases the area of the electrode-electrolyte interface, leading to the development of a large number of surface sites per unit area and EDL, thus directly enhancing the pH sensitivity.³⁶

The interaction of ions with the surface of internal pore walls changes the electric field in the buffer solutions, which in turn changes the electrical sensitivity of the sensing electrode. This interaction is also applied at solid-liquid convergence areas (in Schottky junctions).³⁷ Moreover, the sensitivity of the pH sensing electrode depends on the alteration in the charge distribution within the crystallites due to ion alignment on the surface and ion orientation in the porous layer surface.¹⁸ Moreover, the charge-transfer reactions depend on the shape of the surface due to the effect on adsorption and oxidation of molecules in the p-Si layer.³⁸

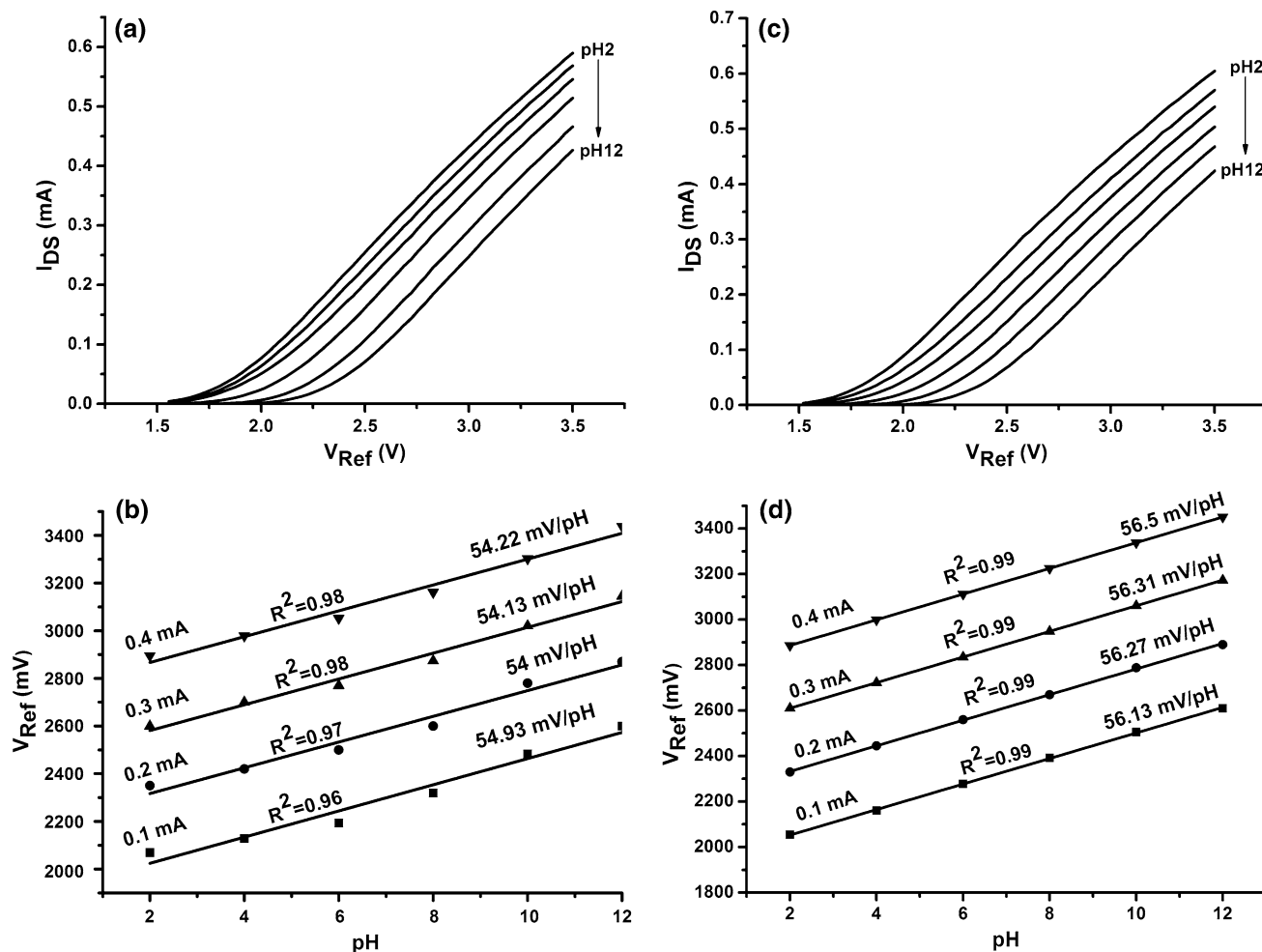


Fig. 8. I_{DS} - V_{Ref} characteristics of EGFET with p-Si for two immersion periods of 60 s and 300 s: (a) I_{DS} - V_{Ref} characteristic for 60 s, (b) V_{Ref} -pH characteristic for 60 s, (c) I_{DS} - V_{Ref} characteristic for 300 s, and (d) V_{Ref} -pH characteristic for 300 s.

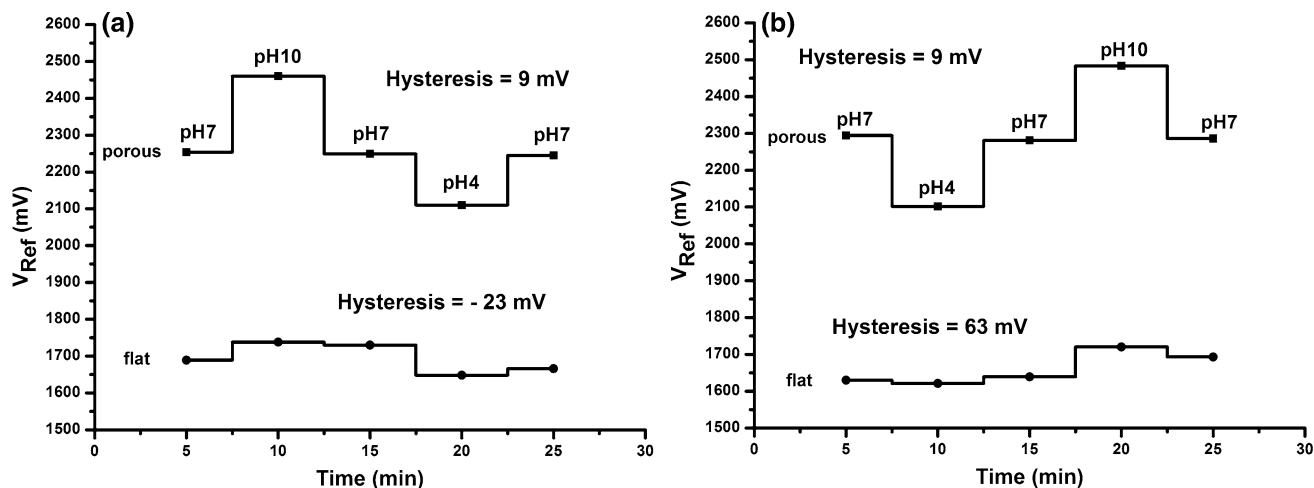


Fig. 9. Hysteresis widths of the two samples in the loop (a) pH 7-10-7-4-7 and (b) 7-4-7-10-7.

Figures 7b, d and 8b, d show the change of the sensitivity for several I_{DS} values. The buffer solutions applied contain many different cations (such

as potassium and sodium) at different concentrations. When the gate voltage changes, these cations may influence the sensing signals due to physical

desorption/adsorption at large pores and tops of silicon rods, because of interchange between these cations and hydrogen ions in the Stern layer; thus, a minor difference in pH sensitivity is recorded.³⁹

The pH sensitivity after immersion time of 300 s was improved slightly compared with 60 s. This result is consistent with the study of Guidelli et al.⁵ This slight improvement can be attributed to H⁺ adsorption by water on the surface. H⁺ adsorption/desorption by other compounds in solution improves the reliability of the pH response, depending on the H⁺ concentration in solution (acid or basic).

Figure 9 shows the hysteresis effort for the two sensor samples. Such hysteresis is due to the chemical interaction between ions in the electrolyte and slowly responding surface sites resulting from defects in the membrane.³⁰ The hysteresis analysis involved dipping the two sensor samples in two cycles of pH buffer solutions (pH 7 → 4 → 7 → 10 → 7 and 7 → 10 → 7 → 4 → 7) with duration of 5 min in each. Afterwards, V_{Ref} at drain current of 0.1 mA was measured from the curves and plotted against the immersion time in the pH buffers. The hysteresis was obtained by subtracting the initial V_{Ref} from the final value at pH 7. The hysteresis depth values indicate good stability of the electrodes, which can be attributed to their thickness, amorphous nature, and porosity.⁴⁰ It can be observed that the hysteresis width for the porous electrode (9 mV and 9 mV) was considerably lower than that for the flat surface (−23 mV and 63 mV).

CONCLUSIONS

This study furthers the notion that surface morphology is a major factor enhancing the pH response. Thus, the barbed nature of the pore shape in porous silicon (111) impedes ion flow inside the pores, enhancing the stability of the sensing performance. Use of (111) p-Si as the basis for an EGFET pH-sensor resulted in good linear behavior with higher pH sensitivity of 56.13 mV/pH in the pH range from 2 to 12 compared with the theoretical value of 59.2 mV/pH. Furthermore, the sensitivity of the drain current to pH showed reliable results with linearity in the tested pH range, showing sensitivity not less than that offered by the reference voltage. Analysis of the stability and reversibility of the sensors showed little discrepancy between the final and initial output voltages of less than 9 mV for pH 7. Based on the presented characterization and analyses, such devices can be considered as good chemical sensors, qualified to respond for two immersion times at room temperature. Moreover, their sensitivity to charged molecules can extend use of these devices to biological applications for selective detection of biomolecules. Therefore, such EGFET devices are very promising for use in future applications as chemical and biochemical sensors.

ACKNOWLEDGEMENT

The authors are grateful to the staff of School of Physics, Universiti Sains Malaysia for facilitating this research.

REFERENCES

1. L.T. Yin, J.C. Chou, W.Y. Chung, T.P. Sun, and S.K. Hsiung, *Mater. Chem. Phys.* 70, 12 (2001).
2. D.S. Kim, J.E. Park, J.K. Shin, P.K. Kim, G. Lim, and S. Shojii, *Sens. Actuators B Chem.* 117, 488 (2006).
3. R. van Hal, J. Eijkel, and P. Bergveld, *Adv. Colloid Interface Sci.* 69, 31 (1996).
4. C. Pan, R. Yu, S. Niu, G. Zhu, and Z.L. Wang, *ACS Nano* 7, 1803 (2013).
5. E.J. Guidelli, E.M. Guerra, and M. Mulato, *ECS J. Solid State Sci. Technol.* 1, N39 (2012).
6. S.M.J. Schöning, A. Kurowski, M. Thust, P. Kordos, J.W. Schultze, and H. Lüth, *Sens. Actuators B Chem.* 64, 59 (2000).
7. S.E. Letant and M.J. Sailor, *Adv. Mater.* 13, 355 (2001).
8. M.J. Sailor, *Porous Silicon in Practice: Preparation, Characterization and Applications* (New York: Wiley, 2012), pp. 104–216.
9. A. Jane, R. Dronov, A. Hodges, and N.H. Voelcker, *Trends Biotechnol.* 27, 230 (2009).
10. J.C. Vial and J. Derrien, *Porous Silicon Science and Technology* (Berlin Heidelberg: Springer, 1995), p. 36.
11. S. Rönnebeck, J. Carstensen, S. Ottow, and H. Föll, *Electrochim. Solid State Lett.* 2, 126 (1999).
12. X.G. Zhang, *J. Electrochem. Soc.* 151, C69 (2004).
13. N. Elfström, R. Juhasz, I. Sychugov, T. Engfeldt, A.E. Karlström, and J. Linnros, *Nano Lett.* 7, 2608 (2007).
14. E.J. Guidelli, E.M. Guerra, and M. Mulato, *Mater. Chem. Phys.* 125, 833 (2011).
15. G. Rong and S.M. Weiss, *Phys. Status Solidi A* 206, 1365 (2009).
16. H. Ouyang, C.C. Striemer, and P.M. Fauchet, *Appl. Phys. Lett.* 88, 163108 (2006).
17. M. Nazari and S. Khatami, *Sens. Mater.* 25, 131 (2013).
18. M. Archer, M. Christophersen, and P.M. Fauchet, *Sens. Actuators B* 106, 347 (2005).
19. J. Fritz, E.B. Cooper, S. Gaudet, P.K. Sorger, and S.R. Manalis, *Proc. Natl. Acad. Sci. USA* 99, 14142 (2002).
20. V. Lehmann and U. Gösele, *Appl. Phys. Lett.* 58, 856 (1991).
21. K. Kunimatsu, *J. Res. Inst. Catal. Hokkaido Univ.* 20, 20 (1972).
22. S. Porada, L. Weinstein, R. Dash, A. van der Wal, M. Bryjak, Y. Gogotsi, and P.M. Biesheuvel, *ACS Appl. Mater. Interfaces* 4, 1194 (2012).
23. P.M. Biesheuvel, Y. Fu, and M.Z. Bazant, *Russ. J. Electrochem.* 48, 580 (2012).
24. K.T. Chu and M.Z. Bazant, *J. Colloid Interface Sci.* 315, 319 (2007).
25. A. Mani and M.Z. Bazant, *Phys. Rev. E* 84, 061504 (2011).
26. F.A. Harraz, *Sens. Actuators B Chem.* 202, 897 (2014).
27. L. Zhang, H. Shen, and J. You, *J. Electron. Mater.* 42, 2464 (2013).
28. C.D. Fung, P.W. Cheung, and W.H. Ko, *IEEE Trans. Electron Devices* 33, 8 (1986).
29. L.L. Chi, J.C. Chou, W.Y. Chung, T.P. Sun, and S.K. Hsiung, *Mater. Chem. Phys.* 63, 19 (2000).
30. A. Das, D.H. Ko, C.H. Chen, L.B. Chang, C.S. Lai, F.C. Chu, L. Chow, and R.M. Lin, *Sens. Actuators B Chem.* 205, 199 (2014).
31. T.M. Pan, M.D. Huang, C.W. Lin, and M.H. Wu, *Sens. Actuators B Chem.* 144, 139 (2010).
32. N.H. Al-Hardan, M.A.A. Hamid, N.M. Ahmed, A. Jalar, R. Shamsudin, O.K. Othman, L.K. Keng, W. Chiu, and H.N. Al-Rawi, *Sensors* 16, 839 (2016).

33. R.R.K. Reddy, A. Chadha, and E. Bhattacharya, *Biosens. Bioelectron.* 16, 313 (2001).
34. M. Thust, M.J. Schöning, S. Frohnhoff, R. Arens-Fischer, P. Kordos, and H. Lüth, *Meas. Sci. Technol.* 7, 26 (1996).
35. F.A. Sabah, N.M. Ahmed, Z. Hassan, M.A. Almessiere, and N.H. Al-Hardan, *JOM* (2016). doi:[10.1007/s11837-016-2165-x](https://doi.org/10.1007/s11837-016-2165-x).
36. P.D. Batista, M. Mulato, C.D.O. Graeff, F.J.R. Fernandez, and F.D.C. Marques, *Braz. J. Phys.* 36, 478 (2006).
37. F.M. Zörgiebel, S. Pregl, L. Römheldt, J. Opitz, W. Weber, T. Mikolajick, L. Baraban, and G. Cuniberti, *Nano Res.* 7, 263 (2014).
38. S. Green and P. Kathirgamanathan, *Mater. Lett.* 52, 106 (2002).
39. Y.H. Lin, C.P. Chu, C.F. Lin, H.H. Liao, H.H. Tsai, and Y.Z. Juang, *Biomed. Microdevices* 17, 1 (2015).
40. W.D. Huang, H. Cao, S. Deb, M. Chiao, and J.C. Chiao, *Sens. Actuators A Phys.* 169, 1 (2011).